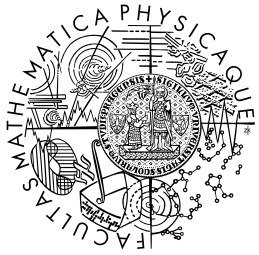

FACULTY
OF MATHEMATICS
AND PHYSICS
Charles University

BACHELOR THESIS

Jan Feireisl

Homoclinic orbits in perturbed black-hole fields

Institute of Theoretical Physics

Supervisor of the bachelor thesis: doc. RNDr. Oldřich Semerák, DSc.
Study programme: FyzikaSS (B0533A110001)
Study branch: FP (0533RA110001)

Prague 2023

I declare that I carried out this bachelor thesis independently, and only with the cited sources, literature and other professional sources. It has not been used to obtain another or the same degree.

I understand that my work relates to the rights and obligations under the Act No. 121/2000 Sb., the Copyright Act, as amended, in particular the fact that the Charles University has the right to conclude a license agreement on the use of this work as a school work pursuant to Section 60 subsection 1 of the Copyright Act.

In ..... date ....

Author's signature

I would like to express my gratitude to my supervisor doc. RNDr. Oldřich Semerák, DSc. for his guidance. I also want to thank my family and friends for their support during my studies, especially Doris Foxová for her emotional support.

Title: Homoclinic orbits in perturbed black-hole fields

Author: Jan Feireisl

Institute: Institute of Theoretical Physics

Supervisor: doc. RNDr. Oldřich Semerák, DSc., Institute of Theoretical Physics

Abstract: In order to generate observable electromagnetic signatures, astrophysical black holes have to interact with matter. Arround the black hole, matter typically forms into a symmetric disc through which it gradually inspirals towards the black hole. If the disc is dense enough, it can significantly perturb the motion of free test particles. The perturbation makes the originally completely integrable dynamical system prone to chaos. In this thesis, we focus on finding the homoclinic orbits which are the 'seeds of chaos' in the geodesic motion around black holes. Specifically, we find the homoclinic orbits in the Schwarzschild and in the extreme Reissner-Nordström space-times, and analyse how they behave under perturbation by a Kuzmin-Toomre disc and by a Majumdar-Papapetrou ring, respectively.

Abstrakt: Astrofyzikální černé díry musí interagovat s látkou, mají-li být pozorovatelné v elektromagnetickém záření. Látka se kolem černé díry typicky uspořádává do symetrického disku, jímž postupně spiráluje k centru. Pokud má tento disk dostatečnou hustotu, může významně ovlivnit pohyb volných testovacích částic. Perturbace změní původně plně integrabilní dynamický systém na systém náchylný k chaosu. V této práci se zaměřujeme na hledání homoklinických orbit, což jsou tzv. „semínka chaosu“ v geodetickém pohybu okolo černých děr. Přesněji hledáme homoklinické orbity v Schwarzschildově a Reissnerově-Nordströmově prostoročasu a zkoumáme jejich chování po superpozici těchto center s Kuzminovým-Toomreovým diskem, resp. Majumdarovým-Papapetrouovým prstencem.

Keywords: general theory of relativity, black holes, geodesic chaos, homoclinic orbits

Contents

Introduction

The study of celestial dynamical systems and their possibly chaotic behaviour all started in 1889 with Henri Poincaré's memoir on the Three body problem [2]. His studies of the N body problem earned him the prize[1] in the contest of King Oscar II. The contest's goal was to answer the question of whether the Solar system is stable or not. Poincaré did not only win the contest but in his analysis he introduced geometrical and topological methods to the study of dynamical systems [21]. Many of Poincaré's methods are still used today (Poincaré section, stable and unstable manifolds, homoclinic points, etc.).

The study of chaos was mostly abandoned until 1963. In this year, Edward Lorenz found out, using numerical simulation, that his model of weather proved to be highly sensitive to change in initial conditions. The advance of computer calculations also provided a precise numerical proof of Poincaré's statements about the stability of the Solar System. We know that even this system, poetically called the 'music of the spheres' and considered to be harmonious, can be highly sensitive to change in initial conditions as proven by Poincaré and the simulations.

With the aid of the relativistic theory of gravitation provided by Einstein, the study of celestial dynamics has since expanded to include the study of black holes, pulsars, accretion discs and neutron stars. The link between non-linearity and chaos makes general relativity prone to chaotic behaviour unless the systems studied are highly symmetric [25]. In this thesis, we will mainly focus on relativistic descriptions of black holes.

By definition, light can not escape from black holes. One thus cannot observe an isolated black hole, but one can observe it's effect on the surrounding matter. The surrounding matter is known to form into larger structures as a result of the gravitational pull of the black hole; this process is referred to as accretion [8]. One of the most well documented structures which is known to form around black holes is the accretion disc. The disc forms from particles which have sufficient angular momentum. The angular momentum prevents the particles from falling straight into the black hole and instead forces them to orbit the black hole. The friction in the disc causes the particles to spiral into the centre. The friction leads to emission of electromagnetic radiation which can be detected. The form of the accretion disc varies depending on the thermal pressure which resists compression.

The mathematics describing black holes usually considers the black hole to be isolated and therefore highly symmetric (no-hair theorems), which leads to the free test-particle motion being integrable and thus non-chaotic. However, even an isolated black hole contains the 'seed of chaos' in the form of the homoclinic orbit. When a perturbation of the isolated black hole occurs, the homoclinic orbit has a tendency to split into a complicated structure called the homoclinic tangle. It was Poincaré who first noticed the peculiar structure of the homoclinic tangle

[1] His original contest winning article had contained a mathematical error which Poincaré discovered after winning. The discovery lead to Poincaré having to pay for the reprinting of the article and him destroying all of the original copies. This historical fact was largely forgotten until 1993 [19].

saying [21]:'One will be struck by the complexity of this figure, which I am not even attempting to draw.' With the perturbation, the symmetry of the isolated system is broken and the motion becomes chaotic. In our study, the perturbation is considered to be caused by an external source, which usually is a disc or a ring, as motivated by astrophysical accretion discs.

This thesis will mainly focus on a) how to mathematically describe chaos, specifically homoclinic chaos, and its emergence in physical systems, b) how to describe free particle motion in isolated and perturbed black-hole fields by using general relativistic formalism, c) finding the homoclinic orbit in isolated and perturbed black-hole space-times.

1. Dynamical Systems

In this chapter, we would like to introduce the reader to basic concepts used in dynamical systems theory which we will then apply in our analysis of relativistic systems in chapters 2 and 3. Rather than delving deep into the abstract formulations, we will attempt to illustrate how the theory applies to our field of study.

1.1 Elementary Definitions

In this thesis, we will define a dynamical system as was done in [6].

Definition 1 (Dynamical system)**.** A dynamical system is defined as a tuple (X, ϕ, T). It consists of the phase space X, a time set $T \subseteq \mathbb{R}$ being an additive semigroup and the time evolution map $\phi : X \times T \to X$ satisfying $\phi(x, 0) = x$ and the group property

$$\phi(x(t_1), t_2) = \phi(x, t_1 + t_2), \tag{1.1}$$

for all $x \in X$ and $t_1, t_2 \in T$.

Unless stated otherwise, we also assume X to be at least a topological space and ϕ to be continuous.

1.1.1 Discrete and real systems

In this thesis, we will mostly work with systems with continuous time. However, in numerical calculations, which are frequently used in chaos theory [6, 31], there is an inherent need for discretisation and we will thus differentiate between systems with continuous and discrete time. Simply put, when the time set T in (Def. 1) satisfies $T \subseteq \mathbb{N}$ we call the dynamical system (X, ϕ, T) discrete and if T is an open interval in the real numbers we call it real.

In practice, we differentiate the two by how the systems time evolution is given. The Chirikov standard map, an example of a discrete dynamical system, uses an iterated map to express time evolution,

$$\begin{aligned} y_{n+1} &= y_n + k \sin(x_n), \\ x_{n+1} &= x_n + y_{n+1}. \end{aligned} \tag{1.2}$$

While a real dynamical system uses a system of differential equations to express time evolution. To give an example we present the differential equation for the mathematical pendulum,

$$\frac{\mathrm{d}^2\theta}{\mathrm{d}t^2} + \frac{g}{\ell} \sin\theta = 0. \tag{1.3}$$

For systems given by differential equations, the solution plays the role of ϕ and is called the flow [31]. Depending on the linearity of the equations describing

the dynamical system, we call the associated system linear or non-linear. Non-linearity is an important feature of chaotic systems [6, 31, 16].

In general relativity, the phase space X is fully described by the metric tensor $g_{\mu\nu}$ and the time evolution is given by the geodesic equation [17]:

$$\frac{\mathrm{d}u^\mu}{\mathrm{d}\tau} + \Gamma^\mu{}_{\alpha\beta} u^\alpha u^\beta = 0. \tag{1.4}$$

τ denotes proper time, u^μ the four-velocity and $\Gamma^\mu{}_{\alpha\beta}$ the affine connection coefficients, which can be computed as Christoffel symbols of the second kind [17]

$$\Gamma^\mu{}_{\alpha\beta} = \frac{1}{2} g^{\iota\mu}(g_{\iota\alpha,\beta} + g_{\beta\iota,\alpha} - g_{\alpha\beta,\iota}). \tag{1.5}$$

Let us stress that the geodesic equation (1.4) only holds for test particles moving freely in the space-time given by $g_{\mu\nu}$. The metric $g_{\mu\nu}$ will be supposed to satisfy the Einstein equations, which is a system of non-linear equations describing how space-time bends via the metric [17]. The equations can be written as

$$G_{\mu\nu} + \Lambda g_{\mu\nu} = \kappa T_{\mu\nu}, \tag{1.6}$$

where $G_{\mu\nu}$ denotes the Einstein tensor, Λ the cosmological constant, κ the Einstein constant and $T_{\mu\nu}$ the energy-momentum tensor. The Einstein tensor is defined as

$$G_{\mu\nu} = R_{\mu\nu} - \frac{1}{2} R g_{\mu\nu}, \tag{1.7}$$

where $R_{\mu\nu}$ is the Ricci tensor and R the Ricci scalar.

1.1.2 Structure of Phase space

The global analysis of a dynamical system can be done by studying the topological qualities of the phase space. In this section, we would like to describe the important structures located in the phase space. Let us illustrate another important concept with the standard map, the concept of a fixed point.

In figure (1.1), we have depicted iterations of the Chirikov standard map (1.2) for different initial conditions. Different initial conditions correspond to different colours in the figure. In the standard map there exist initial conditions for which the evolution "freezes" in one point. These points are called fixed points [6].

Definition 2 (Fixed point)**.** If the equation $\phi(x_s, t) = x_s$ holds for all $t \in T$ in a given dynamical system (X, ϕ, T). Then we call x_s a fixed point.

Definition 3 (Periodic point)**.** If the equation $\phi(x_p, \tau) = x_p$ holds for τ in a given dynamical system (X, ϕ, T). Then we call x_p a periodic point with period τ.

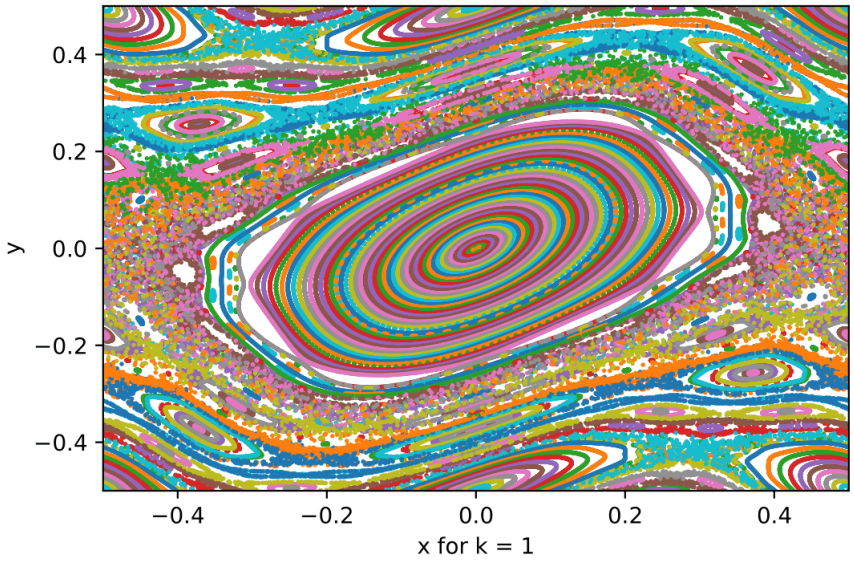

Figure 1.1: Iterations of the Chirikov standard map displayed for different initial conditions.

Note that the periodic point can be viewed as a fixed point given by a new rescaled time evolution map ϕ with a different time parameter τ.

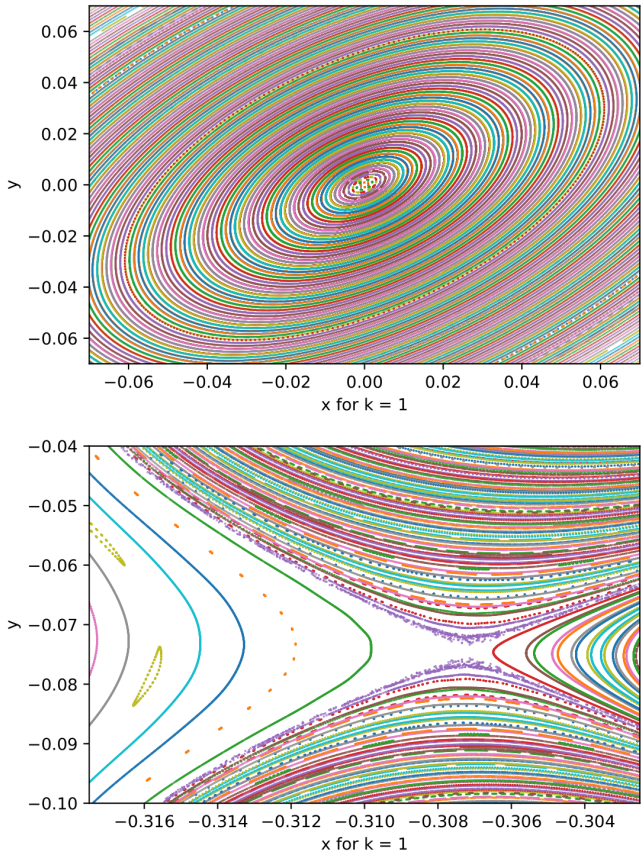

Figure 1.2: (top) Stable fixed point of the standard map (bottom) Unstable fixed point of the standard map.

After looking at the fixed points in detail, we see very different structures near them. In the top figure (1.2), we see a sort of perturbed harmonic oscillator phase space forming around the point. The bottom figure (1.2) shows no such trajectories. Near this fixed point, there are several trajectories being repelled in one direction and attracted towards the point in another. These structures can be investigated using a linear perturbation around a fixed point x_s. For a linear perturbation, we can write

$$\frac{d\delta\mathbf{x}}{dt} = \mathbf{A}(x_s)\delta\mathbf{x}, \tag{1.8}$$

where $\mathbf{A}(x)$ denotes the Jacobian matrix of the time evolution map ϕ. Depending on the eigenvalues of matrix $\mathbf{A}(x)$, where $x \in X$ is given we can determine the stability of the point [15]. In a two dimensional hamiltonian system a simple equation can be obtained for calculating the eigenvalues,

$$\lambda_{1,2} = \frac{\mathrm{Tr}(\mathbf{A}) \pm \sqrt{\mathrm{Tr}(\mathbf{A})^2 - 4}}{2}. \tag{1.9}$$

Definition 4 (Stability classification)**.** Let (X, ϕ, T) be a dynamical system, $x \in X \subseteq \mathbb{R}^2$ a fixed point and $\mathbf{A}(x)$ the Jacobian matrix of ϕ. Let us denote the eigenvalues of $\mathbf{A}(x)$ as λ_1 and λ_2. We also assume the phase space is Hamiltonian. Depending on the trace of $\mathbf{A}(x)$ we call the fixed point x :

1. stable if $\mathrm{Tr}(\mathbf{A}) < 2$,
2. indifferently stable if $\mathrm{Tr}(\mathbf{A}) = 2$,
3. unstable if $\mathrm{Tr}(\mathbf{A}) > 2$.

The eigenvalues are both complex while $\mathrm{Tr}(\mathbf{A}) < 2$ holds (1.9). We can rewrite them as $\lambda_{1,2} = \exp^{\pm i\theta}$. θ can then interpreted as the angular velocity of the points rotating near the fixed point (1.2). This is the reason why it is sometimes referred to as an elliptic point.

If $\mathrm{Tr}(\mathbf{A}) > 2$, then both the eigenvalues are real (1.9). The two eigenvectors correspond to the stable and unstable direction with the interpretation that the trajectories near the point are being pulled inwards in some directions and repelled in others, thus making an unstable equilibrium (1.2). The point is sometimes called hyperbolic.

In order to further classify the topological structures, we need to introduce a new term connected with unstable points. As seen in figure (1.1), we can associate a set of trajectories being repeled or attracted to the unstable fixed point. This set of trajectories defines what we call the (asymptotic) unstable and stable manifolds [31].

Definition 5 (Unstable and stable manifolds)**.** Let x_s be an unstable fixed point in a dynamical system (X, ϕ, T) . We call the set of all points $p \in X$ such that $|\phi^n(p) - x| \to 0$ as $n \to \infty$ denoted by $W^s(x_s)$ the stable manifold of x_s. The unstable manifold of (x_s), denoted by $W^u(x_s)$, is the set of all points $p \in X$ for which $|\phi^n(p) - x| \to 0$ as $n \to -\infty$.

In other words, the stable manifold is the set of all points which asymptotically converge towards the fixed point in the natural flow of time and the unstable manifolds is the set of all points which converge *against* the natural flow of time. Because of the uniqueness of the flow, W^s (W^u) can not cross itself or W^s (W^u) of another fixed point.

With the definitions provided, we can finally get the definition of an important object in our thesis. The intersection of the two manifolds gives us a homoclinic point. The map which maps the homoclinic point onto another homoclinic point is called the homoclinic orbit. The nature of the intersection has vital importance for the onset of chaos. If the intersection is tangential the two form a single smooth homoclinic manifold, the separatrix, on the other hand if the intersection is transversal they are not able to form the same manifold and this leads to a complicated structure called the homoclinic tangle and the onset of chaos [5, 15], which we will discus in a later part.

If we take the physical meaning of the homoclinic orbit it is an orbit that forms a separatrix between plunging and non-plunging behaviour in black hole fields [13]. A trajectory which starts out (at $t \to -\infty$) near the unstable orbit then diverges and converges back towards it at infinity. We will discuss the unstable orbit in the next chapter regarding the effective potential method.

1.2 Hamiltonian systems

A Hamiltonian system is a system described by Hamilton's function $H(q^j, p^j, t)$ and the time evolution is given by Hamilton's canonical equations

$$\begin{aligned} \frac{\partial H}{\partial q^j} &= -\frac{\mathrm{d}p^j}{\mathrm{d}t}, \\ \frac{\partial H}{\partial p^j} &= \frac{\mathrm{d}q^j}{\mathrm{d}t}. \end{aligned} \tag{1.10}$$

In Hamiltonian systems we call the space of variables the phase space, which is in agreement with our established definition of a dynamical system (Def. 1). The solution to Hamilton's canonical equations (1.10) is called the (Hamiltonian) flow. Hamiltonian systems have various interesting mathematical qualities one of them is symplecticity. Symplecticity can be expressed as the Liouville theorem which states that the volume of the phase space is conserved under the flow (1.10).

Moving on from the classical definitions to general relativity for a given metric $g_{\mu\nu}$, we define the Hamiltonian of a free test particle as [17]:

$$H = \frac{1}{2} g^{\mu\nu} p_\mu p_\nu, \tag{1.11}$$

where p_μ is the four-momentum of the particle. Due to the normalisation of four-momentum for massive particles, the equation (1.11) is, in geometrized units[1],

[1] In this unit system, the speed of light and the gravitational constant are set to one, $c = 1, G = 1$. We will exclusively use these units as it is standard in relativistic literature.

equal to $-\frac{1}{2}$ along the actual wordline.

1.2.1 Poincaré map

In general relativity, the phase space is considered 8 dimensional. The conservation of energy can reduce the phase space to a 7 dimensional hypersurface [20]. This makes making graphs of the phase space cumbersome and we thus need to restrict ourselves to a so-called Poincare section which has a codimension of 1 with the original phase space [6].

The section is very frequently defined to make use of the symmetries of the system. As an example, mapping when a particle intersects the equatorial plane [25]. We can get a good idea of what a Poincaré section looks like from a graphical demonstration.

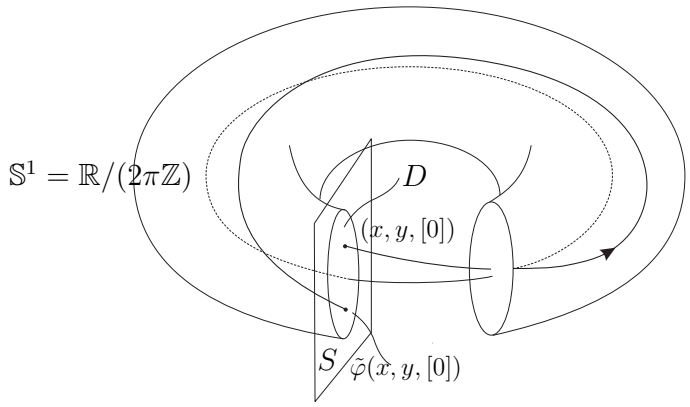

Figure 1.3: Poincaré section of a toroidal phase space, taken from [6].

1.3 Chaos

We will use the definition of chaos provided by Devaney [7].

Definition 6 (Chaotic map (system))**.** Let X be a metric space. The continuous map $\phi : X \to X$ is said to be chaotic on X if:

- ϕ is topologically transitive,
- the periodic points of ϕ are dense in X,
- ϕ has a sensitive dependence on initial conditions.

In this thesis, we will use the term chaotic system and make the assumption that ϕ in the definition corresponds to a time evolution map of the dynamical system (X, ϕ, T). The formal definition of chaos is an ongoing mathematical problem and even the definition provided here is still debated over [1].

In practical terms, the topological transitivity can be viewed as the inability of the system to be broken down into subsystems which do not interact under ϕ. In even simpler words, everything in the system eventually 'mixes'.

The sensitivity to initial conditions can be viewed as the most well known feature of chaotic systems. It is what most people think chaos means and it is often referred to as the butterfly effect in pop culture. Mathematically we can describe it as follows: $\exists \delta > 0 : \forall x_1(t_0)$ and $0 < \epsilon \ll 1, \exists x_2(t_0) : d(x_1(t_0), x_2(t_0))$ at the same time $\exists t : d(x_1(t), x_2(t)) \geq \delta$.

The function $d(x_1, x_2)$ measures distance between two points in the phase space. In other words, given two arbitrarily close initial conditions the two trajectories are arbitrarily distant from each other after sufficient time t under the evolution given by ϕ. The sensitivity to initial conditions can be quantified using the Lyapunov exponents discussed later.

1.3.1 Smale horseshoe

As stated previously, the homoclinic orbit forms a separatrix in an integrable system. When we perturb the system in a way which leads to the stable and unstable manifolds crossing transversally we give rise to the infamous homoclinic tangle which often leads to chaotic behaviour [15].

The emergence of chaos can be demonstrated with a mathematical construction called the Smale Horseshoe map [31]. The construction of the map is purely mathematical but the implications for physical systems will be clarified later in this section.

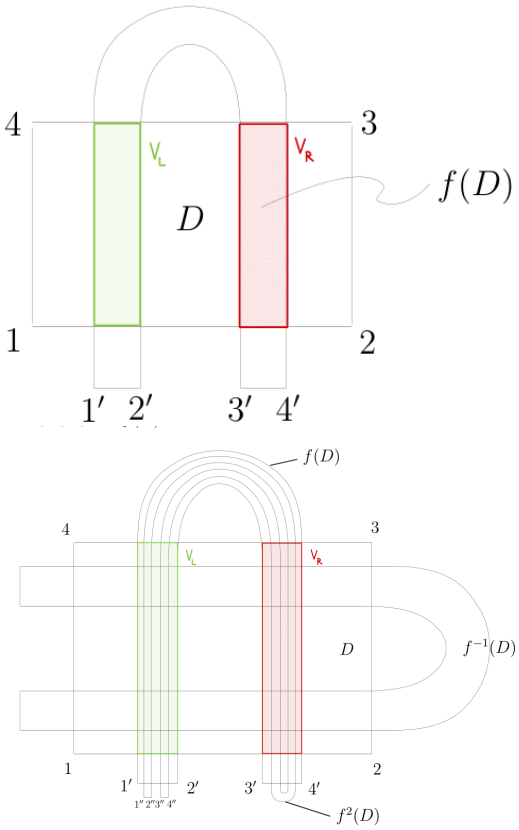

Figure 1.4: (top) Horseshoe map first iteration (bottom) second iteration and inverse Horseshoe map, both taken from [6].

The Horseshoe map is a diffeomorphism $f : \mathbb{R}^2 \to \mathbb{R}^2$ which maps a rectangle D into a horseshoe by stretching in the vertical direction and bending the rectangle [6]. The first two iterations are shown in the figure above. From the figure it can be seen that $D \cap f(D)$ has two components, the two vertical strips. Each of these strips contains two components of $D \cap f(D) \cap f^2(D)$. Using induction we can conclude $D \cap f(D) \cap f^2(D) \cap \cdots \cap f^n(D)$ consists of 2^n vertical strips. We can assign an itinerary to each vertical strip $v \leftrightarrow S_0 S_1 S_2 \dots S_n$ which depends on the location of the strip as follows [31]:

1. if $f^i(v)$ lies in V_L, set $S_i = 0$
2. if $f^i(v)$ lies in V_R, set $S_i = 1$

Note that the strips get thinner with every iteration. If we take the limit of infinitely small strips, the strips reduce to lines and therefore form a Cantor set. We can give each of these lines an infinite address $S_0 S_1 S_2 \dots$.

From figure (1.4), we can find out that the inverse of the Horseshoe map f is again the Horseshoe map, but the whole process is rotated 90°. We have to stretch horizontally and bend the rectangle which intuitively corresponds to the same procedure but rotated. In the limit $n \to \infty$, the procedure reduces the horizontal strips to lines, each of them assigned with an infinite address $\dots S_{-2} S_{-1} S_0$.

If we take the intersection of the two sets of lines and denote it Λ, we get a set of all points that remain in D under all past and future iterations of f. This property makes Λ the so called invariant set of f. Geometrically, this set resembles a "cloud" of points each laying on different intersections of the horizontal and vertical lines. Every point has a unique address expressed in a bi-infinite sequence. $\dots S_{-2} S_{-1} S_0 . S_1 S_2 \dots$

In the field of all bi-infinite sequence Σ, we will define the shift map $\sigma : \Sigma \to \Sigma$ as shifting the itinerary by one spot to the right $S_n \to S_{n+1}$

If we imagine our bi-infinite itinerary as a list of numbers $\dots S_{-2} S_{-1} S_0 . S_1 S_2 \dots$ with a dot between S_0 and S_1. The shift map is equivalent to moving the dot to the right.

$$\sigma(\dots 1001.0101 \dots) = \dots 10010.101 \dots \tag{1.12}$$

We have now transformed the analysis of the system to analysis of bi-infinite sequences of 0 and 1 meaning we have entered the mathematical field of symbolic dynamics. We can see that a periodic orbit in this system evolving according to the shift map looks like an infinitely repeating pattern of 1 and 0. For example an orbit with period two looks like this:

$$P_2 = \dots 0101.0101 \dots . \tag{1.13}$$

There are a countable infinity of periodic orbits of all periods in this system, among them two fixed points ($P_{F1,F2} = \dots 0000.0000 \dots, \dots 1111.1111 \dots$), and an uncountable infinity of non-periodic orbits [31].

Let us take two near initial conditions corresponding to two sequences identical in a block of numbers of length n which we can interpret as n being the maximal number of digits we can determine [2]. The two initially similar conditions can then under a sufficient number of iterations of the shift map be entirely different which is typical behaviour for chaotic systems.

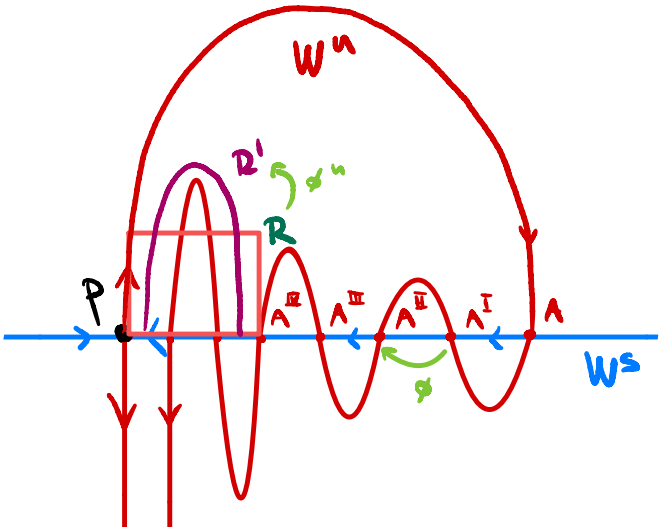

Figure 1.5: Rough sketch of the homoclinic tangle in a Hamiltonian system, redrawn from figure provided in [5].

The similarities between physical (Hamiltonian) systems and the Smale horseshoe may not be apparent but we will demonstrate how the two are related it as was done in [5]. Let us consider an evolution in a Hamiltonian system given by ϕ and let us assume the map has an unstable fixed point P. We can then define the stable manifold W^s and the unstable manifold W^u. For simplicity let us imagine the time evolution is discrete. A homoclinic point A gets mapped to A^I which under the next iteration gets mapped to A^{II} in a manner depicted in figure (1.5).

The points A^N get closer and closer to P. However , they cannot get mapped to the same point twice (it would then be trapped in a cycle and unable to approach the fixed point) and cannot get mapped to the point itself, because the fixed point is its own image (2). The points on the stable manifold merely converge towards it in infinite time (5). The symplecticity of a Hamiltonian system demands that the area between W^s and W^u remains constant, which further complicates the entaglement of the two manifolds. If we would look at the preimages and look at the system in reverse time the same conclusions can be made about how the stable manifold also tangles with the unstable manifold.

If we would look at the rectangle R, in the phase space, we can see that as the rectangle evolves it stretches along W^u, because the eigenvalue near the fixed point is larger than one (4), and then needs to contract in the transversal direction to keep the area constant and conserve the volume of phase space. After enough iterations of ϕ we can get a new rectangle R' that will overlap with R. The map

[2]This is vaguely reminiscent of a realistic measurement, limited by the precision of the measuring device.

ϕ^n restricted to R then acts like a Smale horseshoe. This can be more rigorously expressed and proven as the Smale-Birkhoff theorem [10].

The homoclinic tangle has a very complicated structure. We have already shown the chaotic behaviour of the Standard map in figure (1.1). In the next figure, it can be clearly seen that the chaotic sea of dots is located near the tangle. The splitting of the homoclinic separatrix was also studied in relativistic systems [22, 5] using the Melnikov method.

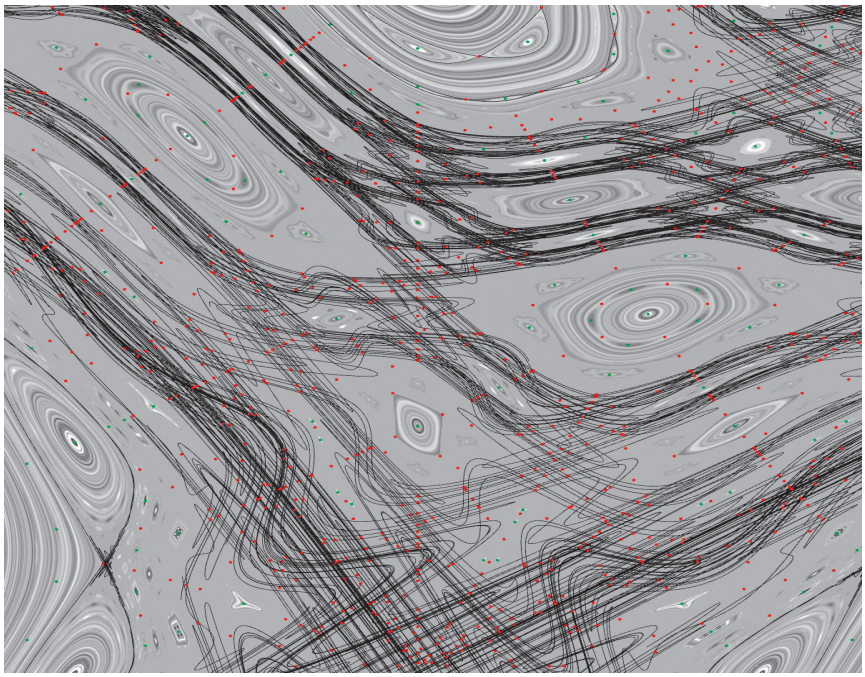

Figure 1.6: Homoclinic tangle of the Chirikov standard map, taken from [28].

1.3.2 Lyapunov exponents

There exist many, usually numerically calculated, coefficients which try to quantify the chaoticity of a system. One of the most important is the (maximal) Lyapunov exponent [6, 31].

Before defining it, we must briefly mention a different view at the sensitivity to initial conditions mentioned in the definition of chaos (Def. 6). For simplicity, lets work with a one dimensional phase space X and a continuous map ϕ as our dynamical system. On this simple phase space imagine two points which are close to each other at time t_0, in mathematical terms x_1 and $x_2 = x_1 + \epsilon$, $\epsilon \ll 1$. Lets define a vector $\boldsymbol{\xi}(t)$ connecting the two near points. We will call this vector the deviation vector. We can interpret the norm of the deviation vector as the distance between the two points at a given time. If the evolution is very sensitive to initial conditions we expect that with time the norm $|\boldsymbol{\xi}(t)|$ will increase exponentially meaning that the two trajectories which start out close to each other get separated with exponential speed. We can further generalise this for a general Hamiltonian phase space [15]. The deviation vector belongs to the tangent space to the phase space and can be evolved by the Hamiltonian flow by applying a linear operator $\boldsymbol{\xi}(t) = D_t\boldsymbol{\xi}(t_0)$.

Definition 7 (Maximal Lyapunov exponent)**.** Let (X, ϕ, T) be a dynamical system. $\boldsymbol{\xi}(t)$ is a deviation vector between two linearly near initial conditions and $t, t_0 \in T$. We can then define the maximal Lyapunov exponent L as:

$$L = \max_{\boldsymbol{\xi}(t_0)} \lim_{t\to\infty} \frac{1}{t} \log \frac{|\boldsymbol{\xi}(t)|}{|\boldsymbol{\xi}(t_0)|} \tag{1.14}$$

As stated previously, for chaotic trajectories we expect $|\boldsymbol{\xi}(t)|$ to grow exponentially with time which means that L converges to a value corresponding to the exponent of the exponential growth. In practice, L is usually calculated numericaly and the limit approximated [15].

In general relativity, the principle of general covariance demands that the equations are independent of the choice of coordinates. Moreover, the formalism of relativity considers time as a coordinate, which can be problematic for the Lyapunov exponent. Nonetheless, it was found that the Lyapunov exponents are to some extent coordinate independent [18].

Many other, usually numerically calculated, Lyapunov type coefficients are used [27, 23]. Other numerical methods include recurrence plots [26] and Fourrier analysis of time series [25].

2. Weyl space-time

2.1 Properties of Weyl metrics

Hermann Weyl's solution to Einstein's equations is one of the earliest solutions [9, 29]. In 1917, Weyl showed that if a given region of space-time is static and axially symmetric and if the energy momentum tensor satisfies $T^{\rho}_{\rho} + T^{z}_{z} = 0$ it is possible to introduce coordinates (ρ, z) of cylindrical type (Weyl's coordinates) in which the metric can be expressed as [25]

$$\mathrm{d}s^2 = -\mathrm{e}^{2\nu(\rho,z)}\mathrm{d}t^2 + \mathrm{e}^{-2\nu(\rho,z)}\rho^2\mathrm{d}\phi^2 + \mathrm{e}^{2\lambda(\rho,z)-2\nu(\rho,z)}(\mathrm{d}\rho^2 + \mathrm{d}z^2), \tag{2.1}$$

where ν and λ are functions of only ρ and z, t and ϕ are cyclic coordinates. It is commonly referred to ν as the gravitational potential because it must satisfy the Laplace equation as a result of the Einstein equations (1.6) (assuming a vacuum and $\Lambda = 0$). The Laplace equation is linear and therefore ν superposes linearly. The analogy with Newtonian potential can also be seen by taking the Newton limit of the metric and looking at the time component. It can be shown that $g_{tt} \sim -1 - 2\nu$.

The second metric function λ does not have a straight-forward interpretation. The function does not superpose linearly but it can be computed by evaluating the following quadratures for a given ν [9]

$$\begin{aligned} \lambda_{,\rho} &= \rho({\nu_{,\rho}}^2 - {\nu_{,z}}^2), \\ \lambda_{,z} &= 2\rho\nu_{,\rho}\nu_{,z}. \end{aligned} \tag{2.2}$$

The fact that ν superposes linearly and λ can be evaluated (2.2) gives us a procedure for the superposition of different static axially symmetric solutions. We take two solutions to the Laplace equation $\nu_{1,2}$ which correspond to the Newtonian solution and superpose their potentials $\nu = \nu_1 + \nu_2$. We can then evaluate λ (2.2). We can interpret the resulting metric as the relativistic analogue of the superposition of two Newtonian solutions.

The first problem of this kind of superposition is that for most cases the λ can only be evaluated numerically. The second problem is that the interpretation can sometimes be tricky. For example, the Minkowski metric, which is the simplest solution to Einstein's equations, has three different corresponding Newtonian potentials ν[9].

2.2 Test particle motion in Weyl space-time

As mentioned before, a free test particle moves in a given space-time according to the geodesic equation (1.4). If we take the Weyl metric (2.1) and compute all of the affine connection coefficients (1.5) and evaluate the terms in the geodesic equation (1.4), we can write [25]

$$\frac{\mathrm{d}u^t}{\mathrm{d}\tau} = -\frac{2\varepsilon}{\mathrm{e}^{2\nu}}(\nu_{,\rho}u^\rho + \nu_{,z}u^z), \tag{2.3}$$

$$\frac{\mathrm{d}u^\phi}{\mathrm{d}\tau} = \frac{2\mathrm{e}^{2\nu}l}{\rho^3}[\rho(\nu_{,\rho}u^\rho + \nu_{,z}u^z) - u^\rho], \tag{2.4}$$

$$\frac{\mathrm{d}u^\rho}{\mathrm{d}\tau} = -\frac{\varepsilon^2\nu_{,\rho}}{\mathrm{e}^{2\lambda}} + \frac{l^2\mathrm{e}^{4\nu}}{\rho^3\mathrm{e}^{2\lambda}}(1-\rho\nu_{,\rho}) + (\nu_{,\rho}-\lambda_{,\rho})[(u^\rho)^2 - (u^z)^2] + 2(\nu_{,z}-\lambda_{,z})u^\rho u^z, \tag{2.5}$$

$$\frac{\mathrm{d}u^z}{\mathrm{d}\tau} = -\frac{\varepsilon^2\nu_{,z}}{\mathrm{e}^{2\lambda}} - \frac{l^2\mathrm{e}^{4\nu}\nu_{,z}}{\rho^2\mathrm{e}^{2\lambda}} - (\nu_{,z}-\lambda_{,z})[(u^\rho)^2 - (u^z)^2] + 2(\nu_{,\rho}-\lambda_{,\rho})u^\rho u^z, \tag{2.6}$$

where $u_t \equiv -\varepsilon$ and $u_\phi \equiv l$ are the two constants of motion implied by the staticity and axial symmetry of the space-time. From the equations (2.3) and (2.4) it would seem like the motion in the (t, ϕ) plane is fully determined by ν, but the components u^t, u^ϕ are coupled with u^ρ and u^z which depend on λ explicitly [25].

2.2.1 Effective potential

In order to examine the motion further, the effective-potential method needs to be discussed. The most known application of this method is the Kepler problem in classical mechanics. The methodology can nevertheless be modified for examining radial motion in general relativity with the same straight-forward graphical interpretation.

Now, we will demonstrate how to use the method for a static and axially symmetric diagonal metric $g_{\mu\nu}$ in the form

$$\mathrm{d}s^2 = g_{tt}\mathrm{d}t^2 + g_{rr}\mathrm{d}r^2 + g_{\theta\theta}\mathrm{d}\theta^2 + g_{\phi\phi}\mathrm{d}\phi^2. \tag{2.7}$$

The symmetries, corresponding to the Killing vector fields ∂_t and ∂_ϕ, give us two constants of motion, the energy $\varepsilon \equiv -u_t$ and the angular momentum $l \equiv u_\phi$ [9]. Let us write down the normalisation of 4-velocity for our metric [17],

$$g^{\mu\nu}u_\mu u_\nu = \varepsilon^2 g^{tt} + (u_r)^2 g^{rr} + (u_\theta)^2 g^{\theta\theta} + l^2 g^{\phi\phi} = -1. \tag{2.8}$$

If we restrict ourselves to circular geodesics in the equatorial plane, we induce the conditions $\theta = \frac{\pi}{2}(u^\theta = 0)$ which further simplifies the expression,

$$\varepsilon^2 g^{tt} + (u_r)^2 g^{rr} + l^2 g^{\phi\phi} = -1. \tag{2.9}$$

Let us further rearrange the terms and use the fact that the metric is diagonal, $g_{\alpha\alpha} = \frac{1}{g^{\alpha\alpha}}$,

$$g_{rr}(u^r)^2 = -\varepsilon^2 g^{tt} - l^2 g^{\phi\phi} - 1, \tag{2.10}$$

$$(u^r)^2 = -\frac{\varepsilon^2}{g_{tt}g_{rr}} - \frac{1}{g_{rr}}\left(\frac{l^2}{g_{\phi\phi}} + 1\right). \tag{2.11}$$

Now, let us define the term on the right as the effective potential,

$$V_{\text{eff}} \equiv \frac{1}{g_{rr}} \left(\frac{l^2}{g_{\phi\phi}} + 1 \right). \tag{2.12}$$

As previously stated, the interpretation is analogous to the Newtonian case. This can best be seen for Schwarzschild and Reissner–Nordström black hole where $\frac{1}{g_{tt}g_{rr}} = -1$ and the expression takes on the familiar form [11]

$$(u^r)^2 = \varepsilon^2 - V_{\text{eff}}^2. \tag{2.13}$$

From the last equation, we see that necessarily $\varepsilon^2 \geq V_{\text{eff}}^2$. Hence, the effective potential represents the minimal value of energy with which a particle of a given angular momentum l can exist at a given location.

Different types of motion can be shown graphically for Schwarzschild space-time. The metric of Schwarzschild space-time can be written as

$$\mathrm{d}s^2 = -\left(1 - \frac{2M}{r}\right)\mathrm{d}t^2 + \frac{1}{1 - \frac{2M}{r}}\mathrm{d}r^2 + r^2(\mathrm{d}\theta^2 + \sin^2\theta \mathrm{d}\phi^2). \tag{2.14}$$

Here we are using Schwazschild coordinates (t, r, θ, ϕ). M is interpreted as the mass of the black hole,[1] r is called the areal radius. It is not the distance from the origin. However, if r and t are held constant with $\theta \in [0, \pi]$ and $\phi \in [0, 2\pi)$, it corresponds to the familiar Euclidean expression $4\pi r^2$ for the surface of a sphere with radius r [9].

Let us return to (2.12) and input the components of the metric tensor for the Schwarzschild black hole (2.14),

$$V_{\text{eff}}^2(r) = \left(1 - \frac{2M}{r}\right)\left(\frac{l^2}{r^2} + 1\right). \tag{2.15}$$

Contrary to the Newtonian case, where a system of a point like massive centre with an orbiting test particle of non-zero l involves an infinite 'centrifugal barrier', the relativistic effective potential always goes to zero at the black-hole horizon. For sufficient values of l, this fact implies the existence of a local maximum of the effective potential. We know that, in analogy to the Newtonian case, a local minimum of V_{eff}^2 produces a stable circular orbit. On the contrary, a local maximum of the effective potential produces a circular orbit that is *unstable*. For completeness, let us mention that the effective potential method can be modified and successfully applied to some non-static space-times, for example the Kerr space-time [20].

[1] The metric itself does not imply any restrictions on the object and the interpretation, it simply describes gravitation around a spherically symmetrically distributed mass in a vacuum. We have written black hole here because it is most relevant to our subject of study.

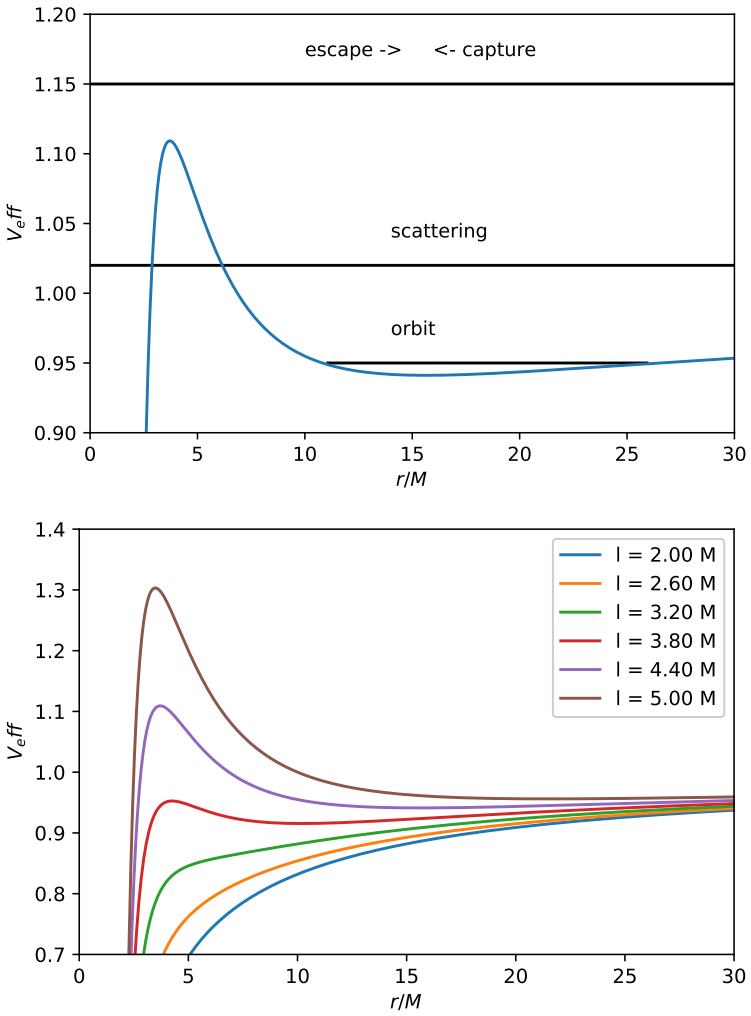

Figure 2.1: (top) Different types of behaviour of massive particles arround a Schwarzschild black-hole, (bottom) effective potential displayed for different values of angular momentum, values chosen in agreement with [3].

For the metric in Weyl coordinates (2.1), we need to slightly modify the definition of V_{eff}^2. If we proceed in a similar fashion as when we derived the equation for equatorial motion $\theta = 0 \Leftrightarrow z = 0$ ($u^z = 0$), we can get to a similar expression to (2.10)

$$\mathrm{e}^{2\lambda}(u^\rho)^2 = \varepsilon^2 - \mathrm{e}^{2\nu}\left(1 + \frac{\mathrm{e}^{2\nu}l^2}{\rho^2}\right). \tag{2.16}$$

The effective potential can then be defined as follows:

$$V_{\text{eff}}^2 \equiv \mathrm{e}^{2\nu}\left(1 + \frac{\mathrm{e}^{2\nu}l^2}{\rho^2}\right). \tag{2.17}$$

The resulting effective potential was also derived in [14] using Lagrangian formalism.

2.2.2 Homoclinic orbits

Let us connect our information about dynamical-system theory, from the first chapter, to our analysis of free test particle motion in black-hole fields. Using the classification (Def. 4), the unstable circular orbit can be classified as a (hyperbolic) unstable fixed point with which the stable and unstable asymptotic manifolds (Def. 5) are associated. The intersection of these manifolds creates a homoclinic orbit. From the definition of the two manifolds, we can gather that the homoclinic orbit approaches the unstable circular orbit in both the infinite future and past. The homoclinic orbit therefore has to have the same ε as the unstable circular orbit.

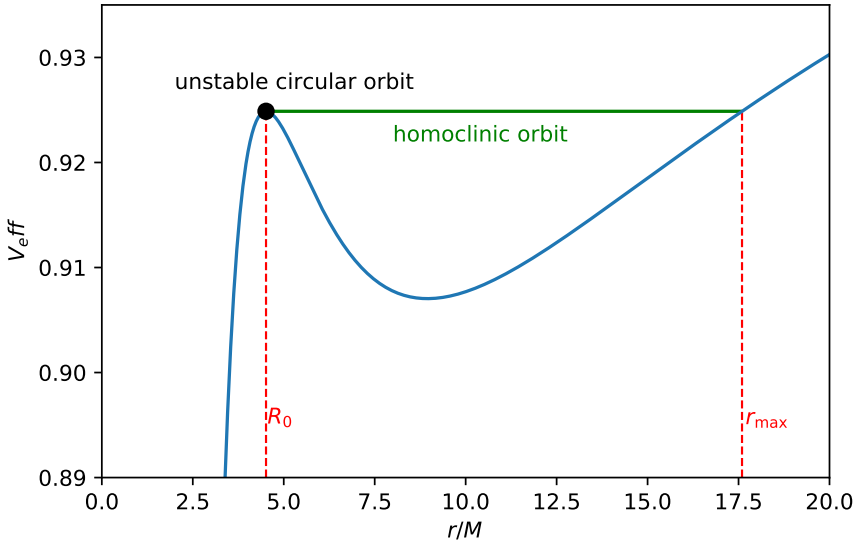

Figure 2.2: Relation of the homoclinic orbit to the effective potential (blue line) in Schwarzschild space-time with highlighted turning points R_0 and $r_{\max}$, for $l = 3.669M$.

The effective potential itself allows us to find the ε of the homoclinic orbit for a given l by finding the local maximum. The equation (2.13) can then be used to determine its shape. Let us first discus the analytic procedure for finding the homoclinic orbit in Schwarzschild space-time. Later, we will try to replace the analytical procedure with a numerical procedure, which can be used for more complicated systems.

Homoclinic orbit in Schwarzschild space-time

Let us restate the form of the equations,

$$(u^r)^2 = \varepsilon^2 - V_{\text{eff}}^2, \tag{2.18}$$

$$V_{\text{eff}}^2(r) = \left(1 - \frac{2M}{r}\right)\left(\frac{l^2}{r^2} + 1\right). \tag{2.19}$$

The first of these (2.18) can also be written in terms of the so-called reciprocal radius, which is defined as $u \equiv \frac{1}{r}$. We want to obtain an equation for u as a function of ϕ. This will allow us to plot the spatial picture of the orbit. For u, the following relation can be derived [25]

$$u^r \equiv \frac{\mathrm{d}r}{\mathrm{d}\tau} = \frac{\mathrm{d}r}{\mathrm{d}u}\frac{\mathrm{d}u}{\mathrm{d}\phi}\frac{\mathrm{d}\phi}{\mathrm{d}\tau} = -l\frac{\mathrm{d}u}{\mathrm{d}\phi}. \tag{2.20}$$

This allows us to rewrite the radial equation into the Binet formula

$$\left(\frac{\mathrm{d}u}{\mathrm{d}\phi}\right)^2 = \frac{\varepsilon^2 - V_{\text{eff}}^2}{l^2}. \tag{2.21}$$

Solving this differential equation will be our main focus in this section. The equation can be used to find the trajectory of a general orbit but we will now restrict ourselves to homoclinic ones. As discussed previously, the homoclinic-orbit energy corresponds to the value of $V_{\text{eff}}^2(r)$ at its local maximum. In order to find the value, we need to differentiate the effective potential with respect to r and set it to 0. This results in the following equation for the stationary points:

$$\frac{\mathrm{d}V_{\text{eff}}^2}{\mathrm{d}r} = 0 \quad \Leftrightarrow \quad l^2 = \frac{Mr^2}{r-3M} \quad \Rightarrow \quad R_0 = \frac{l}{2M}(l - \sqrt{l^2 - 12M^2}), \tag{2.22}$$

where the last implication does not work both ways because we have selected only the root which leads to $V_{\text{eff}}^2(R_0)$ being maximal. In terms of the reciprocal radius, we will define $U_0 \equiv \frac{1}{R_0}$. Let us now further work with (2.21). For a homoclinic orbit, we can write

$$\left(\frac{\mathrm{d}u}{\mathrm{d}\phi}\right)^2 = \frac{V_{\text{eff}}^2(R_0) - V_{\text{eff}}^2(u(\phi))}{l^2}, \tag{2.23}$$

where we have used the same notation as in [22]. The first term on the right hand side of this equation can be further expressed as:

$$V_{\text{eff}}^2(R_0) = \varepsilon^2 = \frac{(R_0 - 2M)^2}{R_0(R_0 - 3M)} \tag{2.24}$$

For completeness, let us also mention how to express the other parameters in terms of reciprocal radius

$$l^2 = \frac{M}{U_0(1 - 3MU_0)}, \tag{2.25}$$

$$V_{\text{eff}}^2(u) = (1 - 2MU_0)(1 + l^2u^2). \tag{2.26}$$

If we return to the Binet formula and substitute in all of the expressions in terms of the reciprocal radius, we can factorise the equation using the fact that U_0 is

a turning point and therefore is a root of the right-hand side. Another root can be found using the fact that $V_{\text{eff}}^2(r)$ reaches the 'homoclinic' energy twice, which can be seen from (2.2). Let us label this second root $r_{\max}$ and define $u_{\max} \equiv \frac{1}{r_{\max}}$. The whole right hand side of the Binet equation can therefore be factorised as follows:

$$\left(\frac{\mathrm{d}u}{\mathrm{d}\phi}\right)^2 = 2M(u-U_0)^2(u-u_{\max}). \tag{2.27}$$

This differential equation has an analytical solution in the form

$$u(\phi) = u_{\max} + (U_0 - u_{\max}) \tanh^2\left[\frac{1}{2}\phi\sqrt{2M(U_0-u_{\max})}\right]. \tag{2.28}$$

The spatial picture of the homoclinic orbit $r(\phi)$ can be then obtained as $\frac{1}{u(\phi)}$.

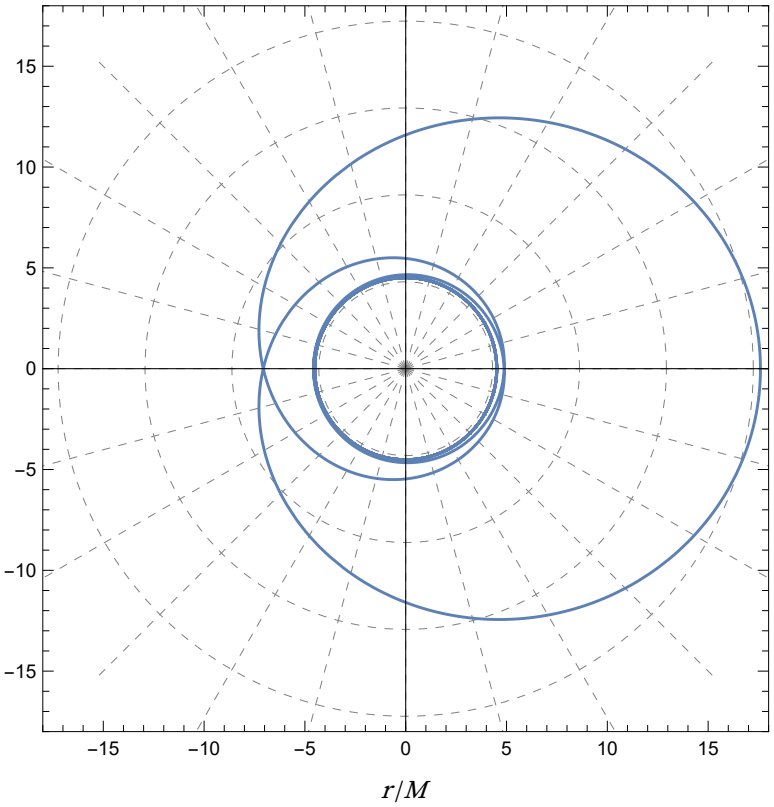

Figure 2.3: Spatial picture of the homoclinic orbit in Schwarzschild space-time, for $l = 3.669M$.

In conclusion, we have managed to replicate the results in [22] and demonstrated a procedure for obtaining the trajectory of the homoclinic orbit in a simple system (Schwarzschild).

Homoclinic orbit in a perturbed field

Now, we wish to use the same procedure for perturbed fields. By perturbed fields, we mean a Weyl superposition of an isolated black hole like Schwarzschild

or Reissner–Nordström space-time and an external source, such as a disc or a ring. Both of the fields can be described by Weyl metric functions ν, λ and therefore can be superposed in a manner described earlier (2.2).

Let us now consider the Schwarzschild black hole as the unperturbed source and a general[2] perturbation which can be described in terms of Weyl metric functions. If we take the Schwarzschild black hole and perform the Weyl superposition with the external perturbing source (in Weyl coordinates), we can obtain a metric describing the compound system. The resulting metric of the system can then be expressed in Schwarzschild coordinates (t, r, ϕ, θ) as follows [25]:

$$\mathrm{d}s^2 = -\left(1 - \frac{2M}{r}\right) e^{2\hat{\nu}} \mathrm{d}t^2 + \frac{e^{2\hat{\lambda}-2\hat{\nu}}}{1-\frac{2M}{r}} \mathrm{d}r^2 + r^2 e^{-2\hat{\nu}} \left(e^{2\hat{\lambda}} \mathrm{d}\theta^2 + \sin^2\theta \mathrm{d}\phi^2\right), \quad (2.29)$$

where the function $\hat{\nu}$ is defined as the ν of the perturbation and $\hat{\lambda}$ is defined as $\hat{\lambda} = \lambda_{\mathrm{P}} - \lambda_{\mathrm{Schw}}$, where λ_{Schw} is the metric function describing the isolated (Schwarzschild) black hole. We will discuss more about the Weyl coordinate description of the Schwarzschild black hole at the end of this chapter.

We will once again look at the motion in the equatorial plane $\theta = \frac{\pi}{2}$ and use the four-velocity normalisation, which will lead to a similar looking radial equation

$$e^{2\hat{\lambda}}(u^r)^2 = \varepsilon^2 - V_{\mathrm{eff}}^2, \quad (2.30)$$

where the effective potential is defined differently than in Schwarzschild space-time[3]

$$V_{\mathrm{eff}}^2 \equiv \left(1 - \frac{2M}{r}\right)\left(1 + \frac{\mathrm{e}^{2\hat{\nu}} l^2}{r^2 \sin^2\theta}\right) \mathrm{e}^{2\hat{\nu}}. \quad (2.31)$$

By using the reciprocal radius we can modify the Binet formula (2.21) to fit a perturbed Schwarzschild black hole,

$$\left(\frac{\mathrm{d}u}{\mathrm{d}\phi}\right)^2 = \frac{\varepsilon^2 - V_{\mathrm{eff}}^2}{e^{2\hat{\lambda}} l^2}. \quad (2.32)$$

At this point, one might be deceived by the likeness of the expressions to that derived for an isolated Schwarzschild black-hole, but we should stop ourselves before jumping to conclusions because several complications are added by the additional source. The first main complication is that the effective potential can have many non-trivial additional terms hidden in $e^{2\hat{\nu}}$. The second complication

[2]The perturbation is not completely general, because, as mentioned before, the class of Weyl metrics considers only static and axisymmetrical fields. This for example excludes a rotating disc or ring, which might be somewhat 'astrophysically disappointing'. Most observed black holes and their accretion disc do in fact rotate as a result of the conservation of angular momentum after a gravitational collapse.

[3]For equatorial motion $\sin^2\theta = 1$.

is that the modified Binet equation contains the second metric function and therefore potentially many terms hidden in $e^{2\hat{\lambda}}$. Note that here, we did not make any assumptions about the metric functions of the perturbation.

Let us nonetheless try to repeat the same procedure as was done in Schwarzschild and attempt to find the stationary points of V_{eff}^2,

$$\frac{\mathrm{d}V_{\text{eff}}^2}{\mathrm{d}r} = 0 \quad \Leftrightarrow \quad l^2 = e^{-2\hat{\nu}} \frac{r^2[r\hat{\nu}_{,r}(r-2M)+M]}{r-3M-2r\hat{\nu}_{,r}(r-2M)}. \tag{2.33}$$

Here, we were able to express l^2 but note that an expression for R_0 can not be expressed from it in the same way as in Schwarzschild. In other words, for a 'generally' perturbed Schwarzschild field, one cannot find the maximum of the potential (the energy of the homoclinic orbit) ε and its position R_0 analytically. However if we consider numerical calculations, the finding of these values should not be difficult because the effective potential, if plotted for 'small amounts' of perturbation[4], looks very similar to the Schwarzschild effective potential. The second turning point $r_{\max}$ can be found by solving the equation $V_{\text{eff}}^2(r) = \varepsilon^2$ and considering only the larger solution $r_{\max} > R_0$.

Assuming we have a value for the energy of the homoclinic orbit, its position R_0 and the second turning point $r_{\max}$, we need to return to the Binet formula, where once again complications arrise. The equation, in a general case, may not be solvable analytically and in a lot of cases we need to once again resort to numerical methods.

With this motivation, let us briefly discuss our numerical procedure for finding the homoclinic orbit. In this thesis, the Wolfram Mathematica function FindMaximum is used for finding the maximum of V_{eff}^2. The function selects a method based on the problem and given an initial guess it finds the maximum ε^2 and its position R_0 with desired precision. The second turning point $r_{\max}$, the larger solution to the equation $V_{\text{eff}}^2(r) = \varepsilon^2$, is obtained using the either the function NSolve or FindRoot. The differential equation is then solved by using these values and one initial condition by the function NDSolve. For the initial condition, we have found that selecting $u(\phi = 0)$ very close, but not exactly equal, to $u_{\max} \equiv \frac{1}{r_{\max}}$ works well.

For the sake of testing the procedure, we can compare the numerical solution of the homoclinic orbit to the analytically obtained formula both for the (non-perturbed) Schwarzschild space-time (2.3).

[4]The parameter considered small is the mass of the external source.

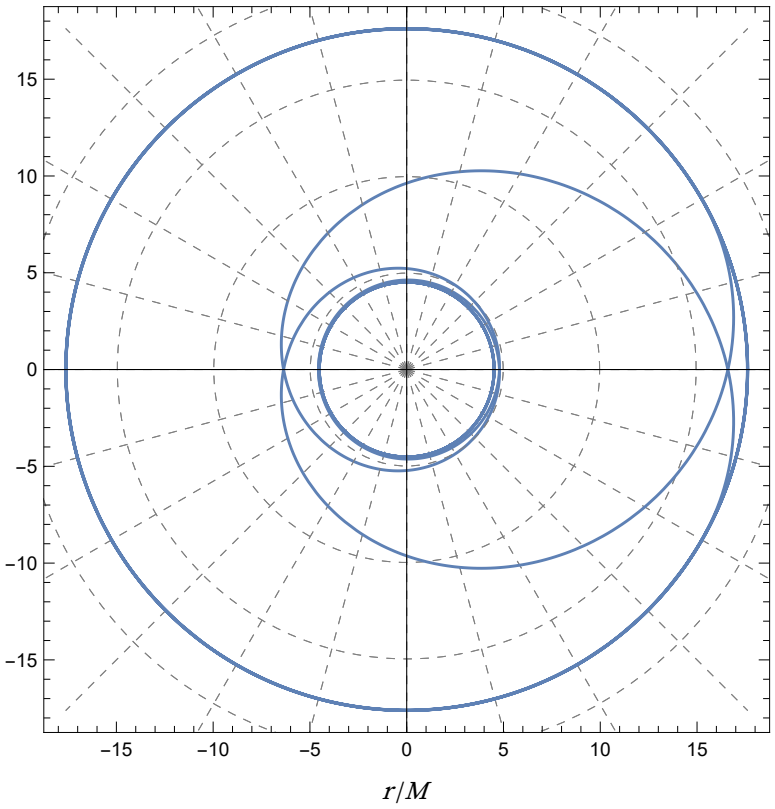

Figure 2.4: Numerical solution for the spatial picture of the homoclinic orbit in Schwarzschild space-time, for $l = 3.669M$.

The main difference occurs near the second turning point $r_{\max}$, where the numerical solution tends to get 'stuck'. From the effective potential, we know that a circular orbit can only exist at a stationary point of V_{eff}^2 and this part of the trajectory should therefore be ignored because it is not physically reasonable. This is the reason why we choose an initial condition slightly offset from the turning point. Nevertheless, the rest of the shape corresponds nicely to the analytically computed orbit (2.3).

2.2.3 Schwarzschild solution as a Weyl metric

The Schwarzschild solution (2.14) can also be expressed in terms of Weyl coordinates (2.1) [25],

$$\begin{aligned} \nu &= \frac{1}{2}\ln\frac{d_1 + d_2 - 2M}{d_1 + d_2 + 2M}, \\ \lambda &= \frac{1}{2}\ln\frac{(d_1 + d_2)^2 - 4M^2}{4\Sigma}, \end{aligned} \tag{2.34}$$

where the functions $d_{1,2}$ and Σ are defined as $d_{1,2} \equiv \sqrt{\rho^2 + (z \mp M)^2}$, $\Sigma \equiv d_1 d_2$. If we look at the expression for the gravitational potential, it corresponds to the Newtonian potential of a finite rod located along the part of the axis $\rho = 0$, with length $2M$ and total mass M [9]. We can now see that the Newtonian analogy is

imperfect, because the original relativistic interpretation of the metric is that of a vacuum spherically symmetric solution [17].

The metric functions can also be written in Schwarzschild coordinates (2.14):

$$\begin{aligned} \nu &= \frac{1}{2}\ln(1-\frac{2M}{r}), \\ \lambda &= \frac{1}{2}\ln\frac{r(r-2M)}{\Sigma}. \end{aligned} \tag{2.35}$$

Schwarzschild coordinates can be transformed back to the Weyl coordinates (2.1) by the relations: $\rho = \sqrt{r(r-2M)}\sin\theta$, $z = (r-M)\cos\theta$.

3. Perturbed black hole fields

In this chapter, we will apply the effective potential method to two perturbed systems, composed of a black hole and an axially symmetric, static perturbation in the form of an external source. After describing basic properties of the perturbing sources, we will compare the resulting effective potentials and the homoclinic orbits in both these systems.

3.1 Kuzmin-Toomre disc

3.1.1 Properties

The inverted Kuzmin-Toomre discs are a class of thin infinitely stretching axially symmetric discs. One of the reasons why these discs generate interest among relativist is that the Newtonian density falls to zero both when the radius (2.1) goes to infinity and when the radius is zero [12]. Therefore, when we consider a superposition with a black hole, there will not be any matter reaching the black hole's horizon and thus necessarily infalling into it's interior.

3.1.2 Metric functions

The discs' Newtonian potential ν is constructed by considering the gravitational effect of a mass distribution $W(b)$ located along the negative part of the axis $z < 0$. The field is then cut at the equatorial plane $z = 0$ and its upper part $z > 0$ is reflected to the negative part $z < 0$ of the axis [12, 4]. The resulting potential is symmetrical when mirrored by the equatorial plane. In cylindrical coordinates (ρ, ϕ, z), the potential is given by

$$\nu = \int_{-\infty}^{\infty} \frac{W(b')\mathrm{d}b'}{\sqrt{\rho^2 + (|z| + b')^2}}. \tag{3.1}$$

The inverted Kuzmin-Toomre discs are then obtained by substituting a combination of the derivatives of the delta distribution, as was done in [4], for the function W and then performing the so-called Kelvin transformation [12]. The potential of the n-th order inverted Kuzmin-Toomre disc can be expressed by the equation

$$\nu_n = -\binom{n + \frac{1}{2}}{n} \frac{M_\mathrm{d}}{(1+2n)!!} \sum_{k=0}^{n} \frac{(2n-k)!}{2^{n-k}(n-k)!}$$

$$\times 2F_1\left(1 + k, k - 1, k - 2n, 2\right) \frac{(-b)^k}{r_b^{k+1}}, P_k(|\cos\theta_b|), \tag{3.2}$$

where $r_b = \sqrt{\rho^2 + (|z| + b)^2}$, $|\cos\theta_b| = \frac{|z|+b}{r_b}$ is the transformation of the cylindrical coordinates ρ and z, $P_k(|\cos\theta_\mathrm{b}|)$ is the Legendre polynomial of degree k evaluated at $|\cos\theta_\mathrm{b}|$, and ${}_2F_1$ is the Gauss hypergeometric function. M_d denotes the mass of the disc.

The second Weyl metric function λ can also be found by using (2.2) and requiring $\lambda \longrightarrow 0$ when $r_b \longrightarrow \infty$ [12],

$$\lambda_{\text{Disc}} = -\binom{n+\frac{1}{2}}{n}^2 \frac{M_{\text{d}}^2 \sin^2\theta_b}{(1+2n)!!^2} \sum_{k,l=0}^{n} \frac{(-b)^{k+l}}{r_b^{k+l+2}} B_{k,l}(n,k,l) P_{k,l}(\theta_b,k,l), \tag{3.3}$$

$$B_{k,l} \equiv \frac{(2n-k)!(2n-l)!}{2^{2n-k-l}(n-k)!(n-l)!(k+l+2)},$$
$$\times {}_2F_1(1+l,k-n,k-2n,2)\,{}_2F_1(1+l,l-n,l-2n,2), \tag{3.4}$$

$$P_k' \equiv \frac{d}{d(\cos\theta_b)} P_k(|\cos\theta_b|), \tag{3.5}$$

$$P_{k,l} \equiv (k+1)(l+1) P_k(|\cos\theta_b|) P_l(|\cos\theta_b|),$$
$$+2(k+1)|\cos\theta_b| P_k(|\cos\theta_b|) P_l'(\theta_b) - \sin^2\theta_b P_k(\theta_b) P_l(\theta_b). \tag{3.6}$$

If we would consider motion in the field of the disc alone, we would come to the conclusion that it does not contain any unstable circular orbits and therefore no homoclinic orbits. Let us move on to the study of the composite system consisting of the Kuzmin-Toomre disc and a Schwarzschild black hole.

3.1.3 Superposition with Schwarzschild black hole

For the form of the metric describing the superposed system, let us refer to the earlier form (2.29). The function $\hat{\nu}$ is defined as the ν of the disc (3.2) and $\hat{\lambda}$ is defined as $\hat{\lambda} = \lambda_{\text{Disc}} + \lambda_{\text{Int}}$. For the Kuzmin-Toomre discs, the metric functions were already listed above. The only new complication, a result of the nonlinearity of general relativity, is that the system's metric function λ is not a simple sum of the two systems' metric functions λ as is the case with ν. A new interaction term λ_{Int} needs to be added.

For the λ_{Int} an iterative expression was derived in [12],

$$\lambda_{\text{Int}}^{(n+1)} = \lambda_{\text{Int}}^{(0)} + \frac{b}{2(n+1)} \frac{\partial}{\partial b} \lambda_{\text{Int}}^{(n)},$$

$$\lambda_{\text{Int}}^{(0)} \equiv -\frac{M_{\text{d}}}{r_b} \left(\frac{d_1}{b+M} - \frac{d_2}{b-M} \right) - \frac{2MM_{\text{d}}}{b^2-M^2}, \tag{3.7}$$

where $d_{1,2}$ are the same functions as in (2.34). The fact that $\hat{\lambda}$ has an analytical expression makes this particular superposed system somewhat unique.

In order to find the unstable circular orbit, we need to restrict ourselves to the equatorial plane again and employ the effective potential method. If we assume that the motion is restricted to the equatorial plane, we have as many constants of motion as degrees of freedom making our system completely integrable. Note that

this is not the case if we are talking about general motion in the superposed field. Non-equatorial motion can be studied by numerical integration of the geodesic equation and studying Poincaré sections [25].

The effective potential can be obtained by using the normalisation of four-velocity and in a way we have already described in the previous chapter (2.31). In the equatorial plane we can write

$$V_{\mathrm{eff}}^2 \equiv \left(1 - \frac{2M}{r}\right)\left(1 + \frac{\mathrm{e}^{2\hat{\nu}} l^2}{r^2}\right)\mathrm{e}^{2\hat{\nu}}. \tag{3.8}$$

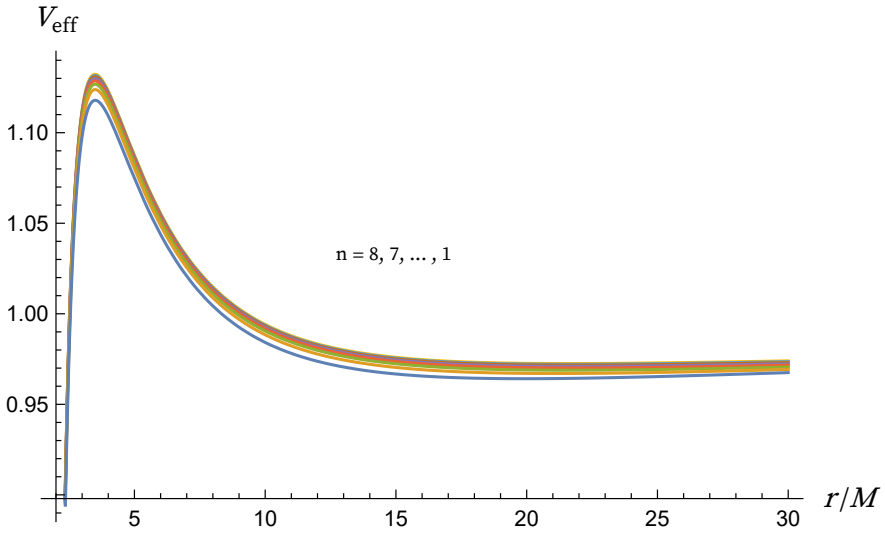

Figure 3.1: Equatorial effective potential of a Schwarzschild black hole encircled by different members n of the Kuzmin-Toomre disc class, constants chosen: $b = 20M$, $l = 5M$, $M_{\mathrm{d}} = 0.5M$. The highest order has the highest local maximum.

For different n, we can see that the plot of the effective potential changes minimally and in result the dynamic properties of the system are not significantly affected. For this reason, in future calculations we will only consider $n = 1$.

3.2 Majumdar-Papapetrou ring

3.2.1 Properties

The Majumdar–Papapetrou (MP) solutions are the only known singularity-free stationary space-times which can describe a system of more than one black hole [24]. In this class of space-times a composite system of charged black holes is maintained in a static equilibrium by their charge. The charge of the black holes has to be extreme[1] $M^2 = Q^2$ in order to compensate for the gravitation pull which is in analogy with classical mechanics. The addition of the electromagnetic field makes the solution, unlike the previous solutions, non-vacuum. For the construction of the MP ring, one needs to consider the field of 'infinitesimal' extremely charged black holes arranged in a circle. The resulting field is

[1]Note that this equality only makes sense in geometrized units.

axisymmetric, static but non-vacuum which is not a problem because the electromagnetic field's energy-momentum tensor is always traceless [17]. This enables us to describe the MP ring in terms of metric functions ν, λ, using Weyl coordinates and superposing it with other Weyl metrics (2.1).

3.2.2 Lapse Function

We should now briefly mention that within the Weyl class of metrics the MP subclass is defined by only having one metric function and $\lambda = 0$ (2.2). The remaining non-zero metric function is referred to as the lapse function, denoted by N and defined as $N \equiv \mathrm{e}^{\nu}$. The metric of this subclass can be written as

$$\mathrm{d}s^2 = -N^2\mathrm{d}t^2 + N^{-2}(\rho^2\mathrm{d}\phi^2 + \mathrm{d}\rho^2 + \mathrm{d}z^2). \tag{3.9}$$

The fact that $\lambda = 0$ makes superposing fields significantly easier because, similarly to ν, as a result of Einsteins equations (1.6) $\frac{1}{N}$ has to be a solution to the Laplace equation and therefore superposes linearly. Both the MP ring and the extreme Reissner–Nordström (RN) black hole fall into this subclass. The lapse function of the MP ring was derived in [24] as

$$\frac{1}{N} = 1 + \frac{2M_{\mathrm{d}}K(k)}{\pi l_2}, \tag{3.10}$$

the terms used in the equation are $K(k)$ denoting the complete elliptic integral of the first kind with $k^2 = 1 - \frac{4b\rho}{(l_2)^2}$ and $l_{1,2} = \sqrt{(\rho \mp b)^2 + z^2}$. b is the Weyl radius of the ring and M_{d} is the ring's mass.

3.2.3 Superposition with Extreme Reissner–Nordström

Reissner–Nordström space-time

The Reissner–Nordström solution is very similar to the Schwarzschild solution (2.14) but the black hole considered has charge. In fact, because of the charge of the black hole the RN solution is not only a solution to Einstein's equations but to Maxwell's equations as well. This makes the field have new interesting properties such as two horizons, more on which can be found in [9, 3]. That being said, the RN metric still shares a lot of properties with Schwarzschild. Namely, it is spherically symetric and static. We will consider an extreme case of parameters, where the charge is equal to the mass of the black hole, as was done when constructing the MP ring, this choice is referred to as the extreme RN black hole and belongs to the MP class. This choice of parameters makes the two horizons merge into one and the field can be described in terms of only one metric function. The lapse function for the extreme RN black hole can be expressed as

$$\frac{1}{N} = 1 + \frac{M}{\sqrt{\rho^2 + z^2}}, \tag{3.11}$$

M denotes the mass of the black hole. The space-time can also be described in Schwarzschild-like coordinates (t, r, ϕ, θ),

$$\mathrm{d}s^2 = -N^2\mathrm{d}t^2 + N^{-2}(r^2\sin^2\theta\mathrm{d}\phi^2 + \mathrm{d}r^2 + r^2\mathrm{d}\theta^2), \tag{3.12}$$

where the relation to Weyl coordinates is necessarily different from Schwarzschild. The transformation has the following form

$$\begin{aligned} z &= (r - M)\cos\theta, \\ \rho &= (r - M)\sin\theta. \end{aligned} \tag{3.13}$$

Superposed system

The superposed system of the RN black hole and the MP ring has a lapse function simply given by the sum of the two systems $\frac{1}{N}$ as

$$\frac{1}{N} = 1 + \frac{M}{\sqrt{\rho^2 + z^2}} + \frac{2M_{\mathrm{d}}K(k)}{\pi l_2}. \tag{3.14}$$

The metric describing the pertubed system can be expressed in the Schwarzschild-like coordinates be substituting the superposed lapse function. For identifying unstable circular orbits and homoclinic orbits, we once again turn to the effective potential method. Using the same procedures and substituting the metric tensor components (**??**), we can write the radial equation and effective potential for a general MP metric,

$$(u^r)^2 = \varepsilon^2 - V_{\mathrm{eff}}^2, \tag{3.15}$$

$$V_{\mathrm{eff}}^2 \equiv \left(1 + \frac{N^2 l^2}{r^2}\right) N^2, \tag{3.16}$$

where it should be emphasised that N is the lapse function of the *composite* system.

3.3 Comparison of perturbed systems.

In this section, we will compare the effective potentials and the homoclinic orbits of the MP ring and RN system and the Kuzmin-Toomre disc and Schwarzschild system. The homoclinic orbit is closely related to the local *unstable* maximum of the effective potential. In Schwarzschild, we saw that this maximum can only occur if the value of l is high enough (2.1). The same tendency is present in both our systems.

3.3.1 Perturbed effective potential

For both our systems, it can be shown that if we take the limit of $M_{\rm d} \longrightarrow 0$ both metric functions approach 1 and the effective potential unsurprisingly reduces to nonperturbed case. In other words, when $M_{\rm d}$ is much smaller than M, the effective potential looks qualitatively like the effective potential of the isolated black hole.

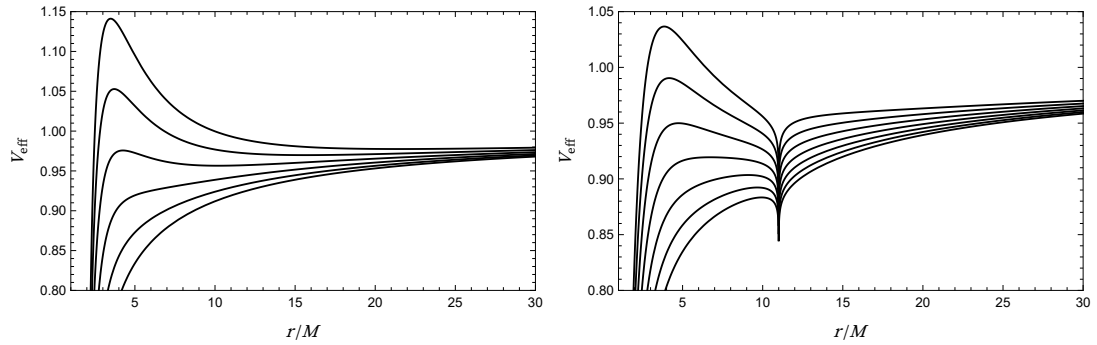

Figure 3.2: Plots of the equatorial effective potential, in Schwarzschild coordinates, for different values of l, (left) for Kuzmin-Toomre and Schwarzschild system with parameters, $b = 20M$, $n = 1$, $M_{\rm d} = 0.01M$ and l ranging from $2M$ to $5M$ (right) for MP ring and RN system with parameters, $b = 10M$, $M_{\rm d} = 0.3M$, l goes from $2.5M$ to $5.5M$.

For the Kuzmin-Toomre composite system, the effective potential has a very similar relation to the changing of l to Schwarzschild (2.31), atleast for M_d small compared to M. We can once again come to the conclusion, that after a certain critical value of l the unstable maximum appears in the graph. The corresponding homoclinic orbit can then be found. In the left column, the figures resemble the plots displayed in [25] for the power-law discs' superposition with Schwarzschild.

The unsmoothness of the figures in the right column (3.2), in comparison to the Kuzmin-Toomre disc superposition, can be explained by considering that the MP ring is a more concentrated source than the infinitely stretching everywhere smooth disc. The new phenomenon, for the MP composite system, is the second local minimum 'valley'. The depth of this 'valley' is dependant on the value of the ring's mass, which is shown in the next set of figures. This new phenomenon only produces a local minimum and therefore does not produce any new homoclinic orbits. Nonetheless, a local maximum still appears for sufficient l.

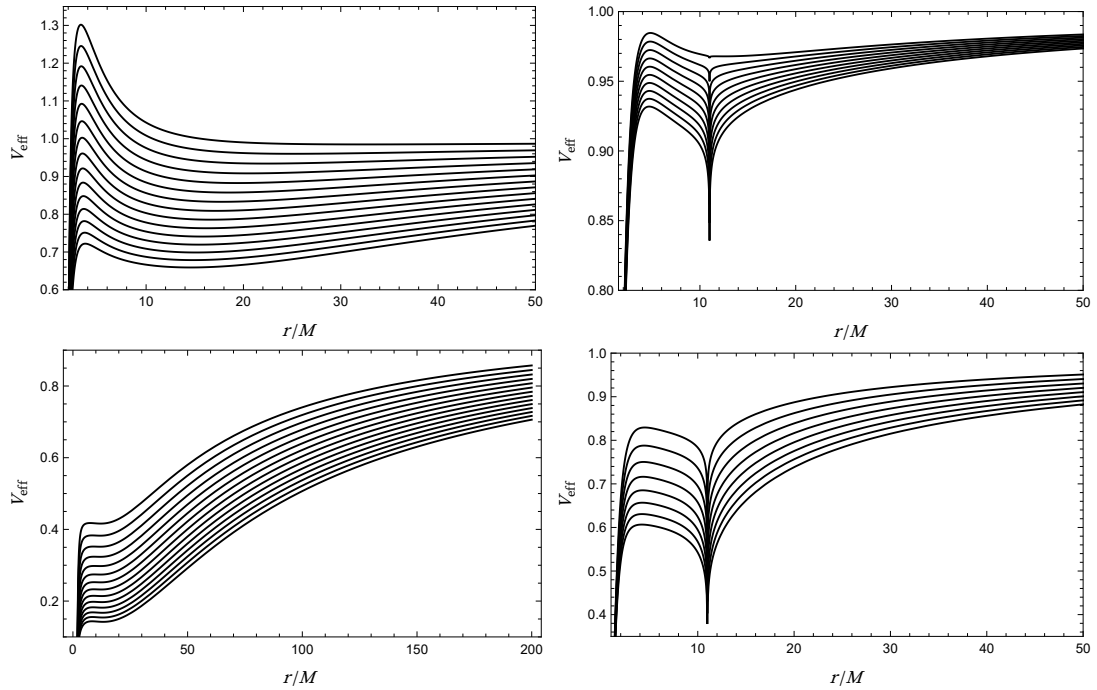

Figure 3.3: Comparison of the relation between mass of the external source M_{d} and the shape of the effective potential in Shcwarzschild coordinates. In the left column displayed for Kuzmin-Toomre disc and Schwarzschild system and in the right column shown for the MP ring and RN system. The values of M_{d} increase as we go from top to bottom. In the left column, the following parameters are constant, $n = 1$, $b = 20M$, $l = 6M$. In the top left M_{d} goes from $0.01M$ to $15M$. In the bottom left, extreme values are chosen, M_{d} goes from $30M$ to $70M$. In the right column, the parameters are chosen as: $b = 10M$, $l = 4.5M$. In the top right, Md goes from $0.01M$ to $0.5M$ and in the bottom right it goes from $1.5M$ to $5M$.

From the figures (3.3), we can conclude that the increase of M_d leads to a decrease in the value of the local maximum. In other words the mass of the external source 'flattens' the effective potential in both systems. If we would compare this effect, the MP ring 'flattens' the function in a more pronounced way. In fact the black hole's field is so strong that the Kuzmin-Toomre disc needs to be unphysically heavy to 'match' its strength. This roughly occurs for values of M_{d} larger than $20M$. For the MP ring composite system, the increase in M_{d} also leads to a deeper 'valley'.

Note that as $r \longrightarrow \infty$, the effective potential necessarily approaches 1 regardless of the value of M_{d}. This might not be apparent from the figure (3.3), especially for very heavy external sources.

3.3.2 Perturbed homoclinic orbits

For both our systems, the Binet formula (2.32) leads us to an equation which can not be solved analytically. In the previous chapter, we have described how to numerically calculate the homoclinic orbit.

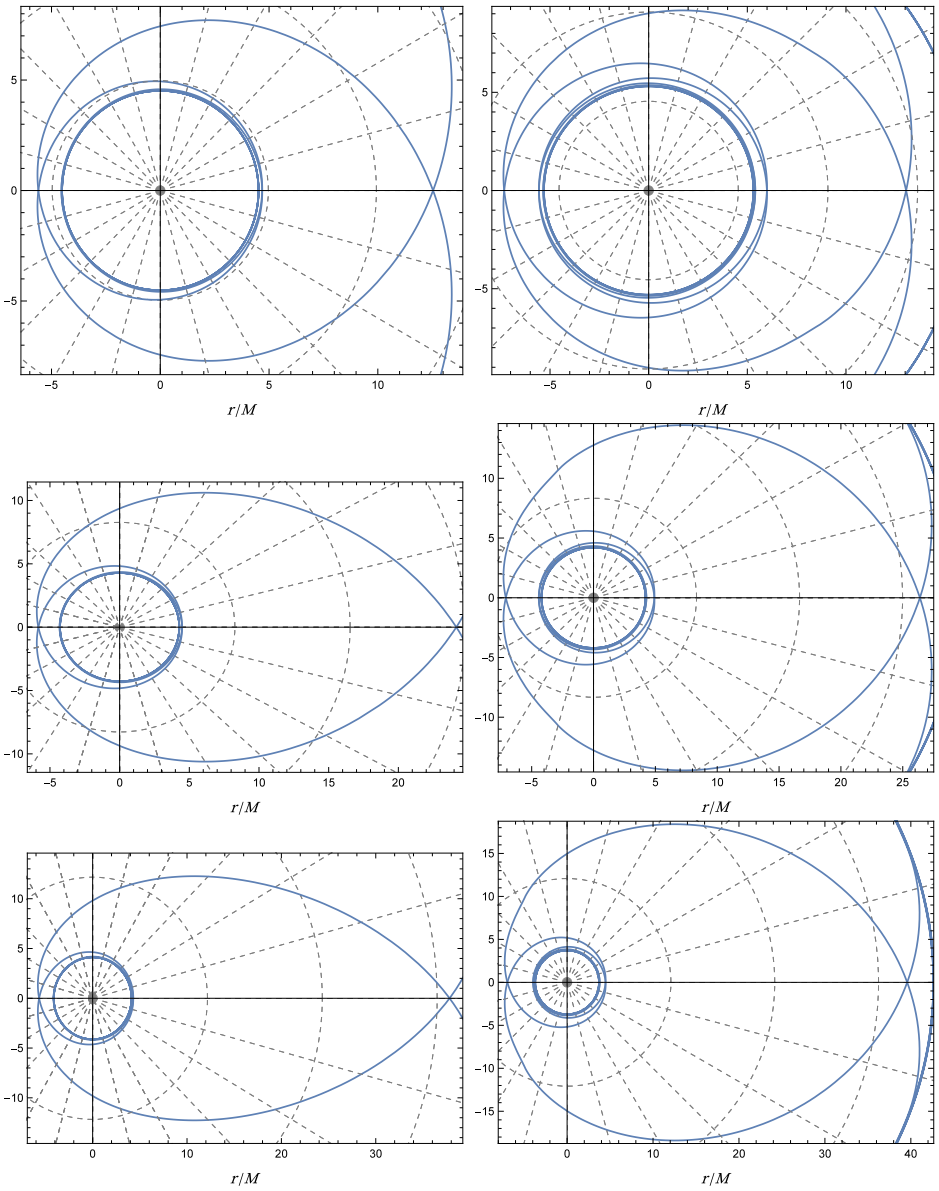

Figure 3.4: Spatial portraits of the homoclinic orbits, in the left column displayed for the first order Kuzmin-Toomre disc and Schwarzschild system and for the MP ring and RN system in the right column. M_{d} increases as we go from top to bottom. In the left column, $b = 10M$ holds for all figures. Similarly, in the right column, $b = 20M$. The remaining parameters l and M_{d} change for every figure. Their values are summarised in the table bellow.

Table: Parameters chosen in figure (3.4). Left two columns of the table corresponds to the left column of the figure and likewise for the right two columns.

M_{d}	l	M_{d}	l
$0.01M$	$3.669M$	$0.1M$	$4.29M$
$0.5M$	$3.828M$	$0.5M$	$4.91M$
$1M$	$3.985M$	$1M$	$5.57M$

For comparison, we have selected parameters that lead to ε^2 being approximately[2] equal for all configurations in a column of figure (3.4). To achieve this, everytime we raise M_d we need to compensate for it by increasing l. In simpler terms, the more the external source flattens the effective potential the more l we need to raise the 'centrifugal barrier'.

In all of the figures, it is apparent that the trajectories approach the unstable circular orbit, which is the defining feature of the homoclinic orbit. Contrary to figure (2.4), we have omitted the second circular orbit, located at the turning point $r_{\max}$, because the existence of this sort of motion at the position is unphysical. Circular orbits can only exist at extrema of the effective potential and thus can not be present at the turning point.

The position of the turning point $r_{\max}$ gets farther away from the horizon as $M_{\rm d}$ increases for both systems. This is a direct result of the flattening done by increasing $M_{\rm d}$. Despite both the systems being different, both have a very similar looking homoclinic orbit. The main difference being that the same increase in $M_{\rm d}$ has a bigger impact for the MP composite system, meaning it's $r_{\max}$ increase more than it would for the same change in $M_{\rm d}$ occuring in the Kuzmin-Toomre composite system.

If we briefly step outside the 'comfort' of integrable equatorial motion and take a look at the meridional plane, which is perpendicular to the equatorial plane, we can get a glimpse of the effect of the Kuzmin-Toomre disc and MP ring on general motion by plotting the effective potential in the $(r\cos\theta, r\sin\theta)$ plane. Let us stress that general motion can not be studied by merely analyzing the effective potential.

In the meridional plan, we need to adjust the radial equation and add back the terms we have previously omitted [30]. For the composite Kuzmin-Toomre disc system, we can write

$$e^{\lambda_P-\lambda}\left[(u^r)^2 + r(r-2M)(u^\theta)^2\right] = \varepsilon^2 - V_{\rm eff}^2, \tag{3.17}$$

$$V_{\rm eff}^2 \equiv \left(1-\frac{2M}{r}\right)\left(1+\frac{{\rm e}^{2\hat{\nu}}l^2}{r^2\sin^2\theta}\right){\rm e}^{2\hat{\nu}}. \tag{3.18}$$

For the MP ring composite system, the λ term vanishes and we can write,

$$\left[(u^r)^2 + r(r-2M)(u^\theta)^2\right] = \varepsilon^2 - V_{\rm eff}^2, \tag{3.19}$$

$$V_{\rm eff}^2 \equiv \left(1+\frac{N^2l^2}{r^2\sin^2\theta}\right)N^2. \tag{3.20}$$

[2]Equal up to three decimal places, for the Kuzmin-Toomre composite system $\varepsilon^2 \approx 0.924$ and for the MP ring and RN system $\varepsilon^2 \approx 0.958$.

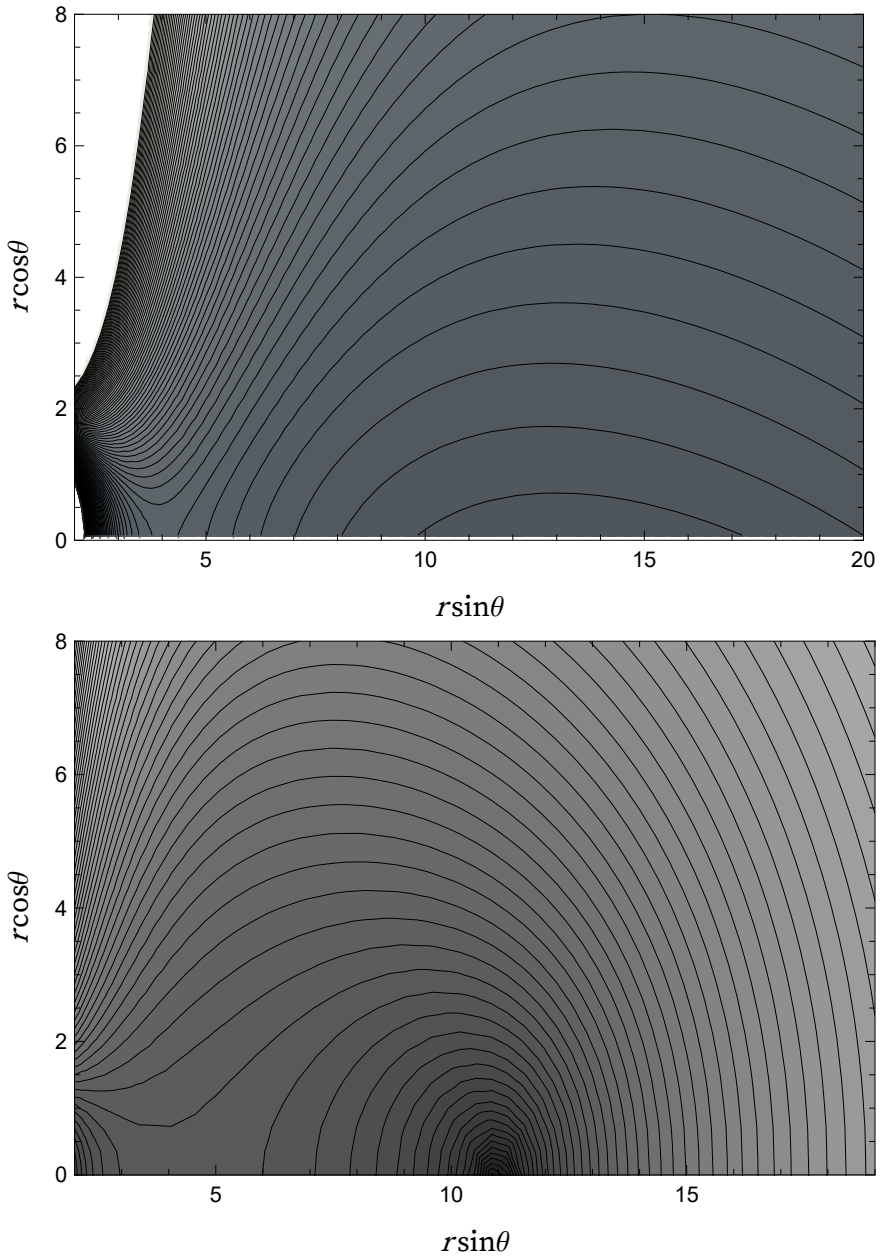

Figure 3.5: Contours of the effective potential displayed in the meridional plane with parameters, (top) for Kuzmin-Toomre composite system with $b = 20M$, $l = 5M$, $M_{\rm d} = 10M$ $n = 1$, (bottom) for MP ring composite system with $b = 10M$, $l = 4.5M$, $M_{\rm d} = 10M$. The choice of $M_{\rm d}$ is highly extreme but it is chosen to clearly illustrate the effect of the sources on the black-hole field.

Conclusion

The main goal of this thesis was to show the importance of homoclinic orbits in (perturbed) black-hole systems. The foundations of chaos theory were summarised and narrowed down to fit our field of study. The onset of chaos was described by the mathematical construction known as the Smale Horseshoe map and the connection to chaos in Hamiltonian systems was shown.

Special attention was paid to axisymmetric, static space-times described by Weyl metrics because they offer a way of superposing metrics. The superpositions were used to perturbe the original black-hole field, destroying the previous integrability of free test-particle motion. The effective-potential method was established. The Binet formula was used to find homoclinic orbits in Schwarzschild field analytically. A simple numerical procedure for finding homoclinic orbits was developed. We applied the procedure to (unperturbed) Schwarzschild space-time and compared the results with the analytic approach. The numerical results reproduced the analytic result almost perfectly.

In this thesis, two composite systems were considered. First, the superposition of the Kuzmin-Toomre disc with the Schwarzschild black hole , and then the system consisting of the RN black hole and the MP ring. In both cases, equatorial geodesic motion was studied and the effective potential method applied in order to find the homoclinic orbit. The effect of the external source's parameters on equatorial geodesics was compared. The numerical procedure proved succesful in finding homoclinic orbits in both systems. The relation between the mass of both sources and the spatial picture of the homoclinic orbits was also discussed.

For a more complete understanding, non-equatorial free-particle motion in both systems should be studied to further analyse the connection between the homoclinic orbits and chaos. The Melnikov method is another possible path for future studies of homoclinic chaos, where the shape of the homoclinic orbits can be utilised.

Bibliography

[1] Banks J. et al., On Devaney's definition of chaos, *The American Mathematical Monthly* 99.4 (1992).

[2] Barrow-Green J., Oscar II's Prize Competition and the Error in Poincaré's Memoir on the Three Body Problem, *Archive for History of Exact Sciences* 48.2 (1994).

[3] Bičák J. and Semerák O., *Relativistic physics*, `http://utf.mff.cuni.cz/~semerak/GTR.pdf`, Lecture notes for a course taught at Prague math-phys, Apr. 2023.

[4] Bičák J., Lynden-Bell D., and Katz J., Relativistic disks as sources of static vacuum spacetimes, *Physical Review D* 47.10 (1993).

[5] Bombelli L. and Calzetta E., Chaos around a black hole, *Classical and Quantum Gravity* 9.12 (1992).

[6] Broer H. W., *Dynamical systems and chaos*, Springer, 2011, p. 313.

[7] Devaney R. L., *An Introduction to Chaotic Dynamical Systems*, Addison-Wesley, 1989, p. 336.

[8] Frank J., *Accretion disk*, `https://www.britannica.com/science/accretion-disk`, July 2023.

[9] Griffiths J. B. and Podolský J., *Exact space-times in Einstein's general relativity*, Cambridge University Press, 2009, p. 525.

[10] Guckenheimer J. and Holmes P., *Nonlinear Oscillations, Dynamical Systems, and Bifurcations of Vector Fields*, Springer New York, 1983.

[11] Hájková T.-M., Homoclinic Chaos in Black-hole Fields, Praha, Bakalářská práce, Univerzita Karlova, Matematicko-fyzikální fakulta, Ústav teoretické fyziky, Vedoucí práce Semerák Oldřich, 2021.

[12] Kotlařík P. and Kofroň D., Black Hole Encircled by a Thin Disk: Fully Relativistic Solution, *The Astrophysical Journal* 941.1 (2022).

[13] Levin J. and Perez-Giz G., Homoclinic orbits around spinning black holes. I. Exact solution for the Kerr separatrix, *Physical Review D* 79.12 (2009).

[14] López-Suspes F. and González G. A., Equatorial Circular Orbits of Neutral Test Particlesin Weyl Spacetimes, *Brazilian Journal of Physics* 44.4 (2014).

[15] Lukes-Gerakopoulos G. and Witzany V., Nonlinear Effects in EMRI Dynamics and Their Imprints on Gravitational Waves (2021).

[16] Meiss J. D., Symplectic maps, variational principles, and transport, *Reviews of Modern Physics* 64.3 (1992).

[17] Misner C. W., Thorne K. S., and Wheeler J. A., *Gravitation*, W. H. Freeman, 1973, p. 1279.

[18] Motter A. E., Relativistic Chaos is Coordinate Invariant, *Physical Review Letters* 91.23 (2003).

[19] Nolte D. D., The tangled tale of phase space, *Physics Today* 63.4 (2010).

[20] Perez-Giz G. and Levin J., Homoclinic Orbits around Spinning Black Holes II: The Phase Space Portrait, *Physical Review D* 79.12 (2008).

[21] Poincaré H., *Les méthodes nouvelles de la mécanique céleste*, Gauthier-Villars, 1892.

[22] Polcar L. and Semerák O., Free motion around black holes with discs or rings: Between integrability and chaos. VI. The Melnikov method, *Physical Review D* 100.10 (2019).

[23] Polcar L., Suková P., and Semerák O., Free Motion around Black Holes with Disks or Rings: Between Integrability and Chaos–V, *The Astrophysical Journal* 877.1 (2019).

[24] Semerák O., Static axisymmetric rings in general relativity: How diverse they are, *Physical Review D* 94.10 (2016).

[25] Semerák O. and Suková P., Free motion around black holes with discs or rings: between integrability and chaos - I, *Monthly Notices of the Royal Astronomical Society* 404.2 (2010).

[26] Semerák O. and Suková P., Free motion around black holes with discs or rings: between integrability and chaos - II, *Monthly Notices of the Royal Astronomical Society* 425.4 (2012).

[27] Suková P. and Semerák O., Free motion around black holes with discs or rings: between integrability and chaos – III, *Monthly Notices of the Royal Astronomical Society* 436.2 (2013).

[28] Tricoche X., Garth C., and Sanderson A., Visualization of Topological Structures in Area-Preserving Maps, *IEEE Transactions on Visualization and Computer Graphics* 17.12 (2011).

[29] Weyl H., Zur Gravitationstheorie, *Annalen der Physik* 359.18 (1917).

[30] Witzany V., Semerák O., and Suková P., Free motion around black holes with discs or rings: between integrability and chaos – IV, *Monthly Notices of the Royal Astronomical Society* 451.2 (2015).

[31] Yorke J. A., *Chaos an Introduction to Dynamical Systems, an Introduction to Dynamical Systems Textbooks in Mathematical Sciences*, Springer-Verlag New York Inc., 2000, p. 622.